RSC Advances

ROYAL SOCIETY OF CHEMISTRY

www.rsc.org/advances

Nitrogen-enriched hierarchical porous carbon with enhanced performance in supercapacitor and lithium–sulfur battery

Xiaoliang Yu [a,c], Jianfeng Zhao [b], Ruitao Lv [b], Qinghua Liang [b], Yu Bai [b], Zheng-Hong Huang [a,b,]*, Wanci Shen [b], Feiyu Kang [b,c,]*

[a] State Key Laboratory of New Ceramics and Fine Processing, School of Materials Science and Engineering, Tsinghua University, Beijing 100084, China

[b] Key Laboratory of Advanced Materials (MOE), School of Materials Science and Engineering, Tsinghua University, Beijing 100084, China

[c] Engineering Laboratory for Functionalized Carbon Materials, Graduate School at Shenzhen, Tsinghua University, Shenzhen 518055, China

E-mail: zhhuang@tsinghua.edu.cn (Z.-H Huang); fykang@tsinghua.edu.cn (F. Kang)

Abstract

It is quite desirable but challenging to prepare highly active materials for various energy storage applications at low costs. Here, an efficient strategy to produce nitrogen-enriched hierarchical porous carbon (N-HPC) is reported by a facile pyrolysis of magnesium citrate and subsequent NH_3 treatment. As-prepared N-HPC presents a developed hierarchical micro- and trimodal meso-porosity with a high specific surface area of 1290 m^2 g^{-1} and pore volume of 3.04 cm^3 g^{-1}. It also shows an abundant nitrogen doping of 3.6%. When used for electrochemical electrodes in supercapacitors and lithium-sulfur (Li-S) batteries, significantly enhanced performances have been obtained comparing with commercially available activated carbon. In supercapacitor testing, the N-HPC electrode shows a specific capacitance of 101 F g^{-1} in nonaqueous electrolyte. And the capacitance retains 67% even at a 200-fold charge/discharge rate. Moreover, its performance in Li-S batteries is more

outstanding. It enables a very high sulfur loading (76.2% by weight) and the resulting

N-HPC/S cathode shows high discharge capacities of 1153 mAh g^{-1}_{sulfur} (or 702 mAh

$g^{-1}_{electrode}$) at 0.2 C and 671 mAh g^{-1} even at 4 C. And it still remains 600 mAh g^{-1}

over 300 charge/discharge cycles at 1 C with an average Coulombic efficiency of

99.0%.

Keywords: Magnesium citrate; Hierarchical porous carbon; Nitrogen-enriched;

Supercapacitor; Lithium-sulfur battery.

Introduction

Among various electrochemical energy-storage devices, supercapacitors and

lithium-sulfur (Li-S) batteries are the two most attractive and promising technologies

due to their ultrahigh power and energy density, respectively.[1-4] Supercapacitors, also

called electrical double layer capacitors, are able to achieve energy uptake and

delivery within seconds through rapid physical ion adsorption/desorption. While

lithium-sulfur (Li-S) batteries can offer a theoretical capacity of 1672 mAh g^{-1} by the

multi-electron-transfer redox reaction between sulfur and lithium.[5] In spite of recent

tremendous advance in these two areas, their commercial application still faces

several challenges. For supercapacitors, it is still a great challenge to develop

electrode materials with high energy and power densities at low costs.[6, 7] While the

application of Li-S batteries is hindered by the low utilization of sulfur due to its

intrinsic insulation, as well as the poor cyclic stability caused by the highly

electrolyte-dissoluble lithium polysulfides and the volume variation during

charge/discharge process.[8-10]

In recent years, hierarchical porous carbons (HPCs) have received considerable attention owing to their chemical stability, good conductivity, and especially their hierarchical porosity combining micropores, mesopores and macropores. These features make them ideal candidates for applications like catalysis,[11] sensors,[12] adsorption and separation.[13] And they also show great advantages for applications in supercapacitors and Li-S batteries.[14-17] In supercapacitors, the micropores provide plenty of electroactive sites to confine the electrolyte ions and store the energy, while mesopores and macropores act as smooth ion diffusion channels for high-rate charge/discharge processing. In Li-S batteries, the carbon framework can serve as effective sulfur-loading matrix and greatly facilitate electron transport. The micropores and small mesopores effectively confine sulfur and suppress the diffusion of polysulfides, meanwhile large mesopores and macropores serve as the transport pathway for ions and improve the ability to withstand volume expansion of sulfur during cycling. Besides, developed meso- and macroporosity enables ample accommodation space for high sulfur loading, which could greatly enhances the overall capacity of the cathode and are thus highly desirable in Li-S batteries.[18, 19] So far, considerable progresses have been made to prepare such HPCs with high porosities. Srinivas et al. synthesized HPCs with simultaneously high surface area and high pore volume through carefully controlled carbonization of in-house optimized metal–organic frameworks (MOFs).[20] Nazar et al. employed porous silica as the hard template to prepare ordered mesoporous carbon nanoparticles with extremely high bimodal porosities.[21] Huang et al. fabricated three-dimensional hierarchical porous

carbon with polypyrrole (PPy) microsheets as precursor and KOH as activating agent.[22] However the above-mentioned synthesis procedures are complicated and high-cost due to the preparation of some precursors like MOFs and hard templates, or the post chemical activation. Thus facile synthesis of such HPCs at low cost is highly desired.

Recent researches also show that surface functional groups play important roles in performance enhancement of the carbon-based electrode materials.[23-26] The heteroatoms such as O, N, B or P in porous carbons enable enhancement of the electrical conductivity, wettability in the electrolyte, and therefore improve the electro-active surface area. In addition, functional carbon-sulfur cathodes show enhanced adsorption of sulfur and lithium sulfide on carbon leading to improved cycling stability.[27, 28] Among various heteroatom doping method, nitrogen doping through NH_3 treatment has been reported to be one of the most effective approach.[29-31]

Citrates are food additives in our daily life. Inagaki firstly adopted magnesium citrate as both carbon source and hard template to prepare mesoporous carbons.[32] After that, several researches have been reported to prepare porous carbons using citrates for various energy storage/conversion applications, like supercapacitor,[33, 34] lithium ion battery,[35] and Li-S battery.[36] In this work, we synthesized nitrogen-enriched hierarchical porous carbon (N-HPC) by finely controlled pyrolysis of magnesium citrate and subsequent nitrogen doping through NH_3 treatment. As-prepared N-HPC shows a unique micro- and trimodal meso-porosity as well as abundant nitrogen functional groups. More importantly, such N-HPC can be

4

simultaneously used for high-performance electrochemical electrodes in supercapacitors and Li-S batteries.

Experimental

Typically, N-HPC was prepared through facile pyrolysis of magnesium citrate and subsequent NH_3 treatment. The pyrolysis was carried out in a tubular furnace under N_2 atmosphere at 220, 350, 435 °C for 1 h and then 850 °C for 2 h with a ramp rate of 2 °C min^{-1}. The product was thoroughly washed with diluted HCl solution and deionized water and then dried at 120 °C to get the hierarchical porous carbon (HPC). Following NH_3 treatment was performed under NH_3 atmosphere at 800 °C for 2 h with a ramp rate of 5 °C min^{-1} to obtain the target N-HPC material. Commercially available activated carbon YP-17D (Kuraray Co., Japan) was used as received in this work for comparison.

Nitrogen-enriched hierarchical porous carbon/sulfur (N-HPC/S) composite was prepared by melt diffusion method. N-HPC was mixed with the sublimed sulfur (99.99% Aladdin) with weight ratios of 1:5, and ground into uniformity. Then, the composite was heated at 155 °C with a ramp rate of 3 °C min^{-1} for 10 h and further treated in a tubular furnace at 300 °C with a ramp rate of 5 °C min^{-1} under N_2 atmosphere for 0.5 h to remove the sulfur on the outer surface. HPC/S and YP-17D/S composites were prepared using the same method.

The weight percentages of sulfur in the carbon/sulfur (C/S) composites were measured by TGA measurement on a TA 2950 instrument. The samples were tested under N_2 atmosphere from 30 °C to 700 °C at a heating rate of 10 °C min^{-1}. The

morphology and microstructure were examined with a scanning electron microscopy

(SEM, LEO-1530) and transmission electron microscopy (TEM, Tecnai G20, 200 kV).

N_2 adsorption isotherms were measured by using a volume adsorption apparatus

(autosorb-1) at 77 K. The total pore volumes were estimated from single point

adsorption (P/P_0= 0.99), the specific surface area was calculated by

Brunauer-Emmett-Teller (BET) method, the micropore surface area and micropore

volume were determined by t-plot method, and pore size distributions (PSD) were

derived from density functional theory (DFT). PHI Quantera Imaging X-ray

photoelectron spectroscopy (XPS) was used to investigate the surface chemistry.

X-ray diffraction (XRD) patterns were obtained from a D8 Advance Diffractometer

(Bruker AXS) with a Cu Kα source.

For supercapacitor electrodes, the porous carbons (N-HPC, HPC and YP-17D)

were mixed with 15% PVDF, 10% carbon black (Super P) and plenty of NMP as

solvent to get a homogeneous slurry. Then the slurry was coated onto a copper foil

and subsequently dried at 80 °C for 4 h and at 120 °C in vacuum for 12 h. While the

working electrode of Li-S batteries were prepared by mixing C/S composite

(N-HPC/S, HPC/S and YP-17D/S) with 10% PVDF and 10% carbon black. The slurry

was coated onto an aluminum foil and then dried at 60 °C for 24 h. The electrodes

were punched into a disk with a diameter of 12 mm for electrochemical tests. The

mass loading of porous carbon electrodes were ~ 1.2 mg, while the mass loading of

C/S composite electrodes were ~ 1.5 mg.

For symmetric supercapacitors, cyclic voltammetry (CV) tests were performed in

6

VSP-300 electrochemical interface with a voltage window of 0-2.7 V. The electrolyte is 1 M $LiPF_6$ in EC/DEC (1:1 by volume). Galvanostatic charge/discharge cycling (GC) measurements were performed in Arbin-BT2000 test station. The specific capacitance of single electrode was calculated according to the formula: $C = 4I\Delta t/(m\Delta V)$, where I is the constant current (A), m is the total mass of the electroactive materials (g), ΔV is the potential change (V) within the discharge time Δt (s). The current densities for GC tests discussed in the context are all based on the average mass of the two electrodes. A LAND battery tester (Jinnuo Electronics Co., Wuhan, China) was used to perform the GC tests of the Li-S batteries with a voltage window of 1.7-2.8 V. The electrolyte was 1.0 M lithium bis(trifluoromethanesulfonyl)imide (LITFSI) in 1,3-dioxolane (DOL) and 1,2-dimethoxyethane (DME) at 1:1 volume ratio with 1 wt% $LiNO_3$ added as an additive. The rate set for Li-S cell tests was referenced to the mass of sulfur active material in the cathode, and 1 C equaled to 1675 mA g^{-1}. Cyclic voltammetry (CV) and electrochemical impedance spectroscopy (EIS) tests were performed in VSP-300 electrochemical interface.

Results and discussion

Scheme 1 illustrates the synthesis procedures of the N-HPC material, which consist of direct pyrolysis of magnesium citrate, acid washing and subsequent NH_3 treatment. During pyrolysis, the organic moiety polymerized and then further carbonized to form the carbon framework, and the magnesium ions nucleated to form nanocrystals of MgO. Acid washing was conducted to remove MgO nanocrystals and produce the mesopores. NH_3 treatment was performed to dope the porous surface with abundant nitrogen functionalities. Fig. S1a. depicted the thermogravimetric analysis of magnesium citrate. In general, the pyrolysis process is characterized by a three-stage thermal degradation. At temperatures below 200 °C the weight loss is due to the

dehydration of magnesium citrate. While at intermediate temperatures (~300–400 °C) the weight loss should mainly be ascribed to the formation of inorganic species (MgO). Finally at high temperatures (~400–500°C), the weight loss comes from the pyrolysis of the organic moiety into the carbon framework. In order to get a stabilized porous carbon framework, we set up the heat treatment procedures according to the TGA curve and conducted isothermal treatment at three knee points (as shown in Fig. S1b).

Scanning electron microscopy (SEM) and transmission electron microscopy (TEM) were used to characterize the microstructure of as-synthesized sample and the results are shown in Fig. 1. From Fig. 1a it can be seen that the carbon particles show an irregular morphology with particle sizes from 2 to 10 μm. From the TEM image in Fig. 1b we can observe plenty of mesopores with uneven pore size from 10 nm to 30 nm. These large mesopores could favor the sulfur impregnation and benefit for the smooth transportation of electrolyte ions during charge/discharge.

Nitrogen adsorption tests were undertaken to further characterize the texture properties of the porous carbon materials. Sample HPC and the commercially available activated carbon YP-17D were also tested for comparison. Fig. 2a and Fig. S2a show the resulting nitrogen adsorption-desorption isotherms and their corresponding pore size distribution (PSD) curves .We can observe that the isotherms of sample N-HPC and HPC exhibit a hybrid of type-I and type-IV isotherms with a capillary condensation step, indicating their dominant mesoporous structures. While YP-17D presents a typical type-I isotherm suggesting its micropore structure. From

8

the corresponding PSD curves, we can see that YP-17D shows a much more developed micropore peak at about 1 nm than those of N-HPC and HPC, while the latter show more enhanced mesoporosities with trimodal distributions centered at 3.8 nm, 8.9 nm and 11.2 nm. The micropores and small mesopores (<7 nm) come from the thermal decomposition of carbon matrix, while large mesopores (10 nm and above) should be ascribed to the voids formed by removal of MgO nanocrystals. The porosity parameters were calculated and summarized in Table S1. We can see that the porosity of YP-17D is mainly contributed by micropores, while sample N-HPC and HPC show much more developed mesoporosities with high total pore volumes of around 3 cm^3 g^{-1}. We can also find that NH$_3$ treatment causes minor change of the porous structure, with little enhancement of specific surface areas and pore volumes, and almost no change of the pore size distributions. XPS analysis were carried out to measure the chemical composition of porous carbons, since the surface chemistry plays an important role in determining their surface polarity and electric conductivity [37-39]. The results are shown in Fig. 2b and Fig. S2b. For sample HPC and YP-17D, only pronounced peaks of C and O elements can be observed. While, additional peak of N element can be detected at ~ 400 eV for sample N-HPC. Based on the XPS quantitative analysis, a nitrogen content of 3.6% was determined for N-HPC. Such abundant nitrogen functionalities are quite beneficial for improving the polarity and wettability of the porous surface as well as enhancing the electric conductivity.

Inspired by the developed hierarchical porosity and high nitrogen content, we employed N-HPC as the supercapacitor electrode. Its capacitive performance was

investigated by assembling symmetric supercapacitors in the $LiPF_6$ electrolyte with

working voltage ranging from 0 to 2.7 V, and the results are shown in Fig. 3. HPC and

YP-17D were also tested for reference. Fig. 3a and Fig. S3 show the cyclic

voltammetry (CV) curves for three porous carbons at various scan rates from 10 mV

s^{-1} to 100 mV s^{-1}. The CV curves of sample N-HPC and HPC exhibit nearly

rectangular shape, indicating the electric-double-layer capacitive (EDLC) behavior.

And they were well retained even at high scan rate (100 mV s^{-1}). While the CV curves

for YP-17D shows some distortion, which becomes more significant as the scan rates

increase. And this should be ascribed to the lack of mesopore diffusion channels and

thus slower ion transport at high rate operations.[40] Galvanostatic charge/discharge

cycling (GC) tests were performed to evaluate the specific capacitance of the

electrodes and the resulting charge/discharge curves are presented in Fig. 3b. The GC

curves are linear and show isosceles triangle shapes. This again suggests the EDLC

feature, and also indicates the high electrochemical reversibility. The specific

capacitances of two porous carbons at various current densities were calculated and

plotted in Fig. 3c. At a low current density of 0.1 A g^{-1}, N-HPC shows a specific

capacitance of 101 F g^{-1} which is a little lower than that of HPC (106 F g^{-1}) and much

higher than 89 F g^{-1} of YP-17D. At a high current density of 20 A g^{-1}, YP-17D retains

only 32% of its capacitance, while the capacitance retentions for N-HPC and HPC are

67% and 53%, respectively. In comparison with those of previously reported

advanced porous carbons, the rate performance of sample N-HPC is still outstanding

(as shown in Fig. S4). Fig. S5 shows the EIS spectra of three porous carbons. In the

low frequency region, the depressed semicircle can be ascribed to the charge transfer process at the electrode/electrolyte interface. The intercept of the semicircle with the real axis equals the electronic resistance (R_e) of the supercapacitor device. The R_e values for N-HPC, HPC and YP-17D can be calculated to be 1.35, 1.74 and 1.92 ohm respectively, indicating the enhanced electronic conductivity by nitrogen doping. At middle frequency, sample YP-17D shows a typical 45° Warburg line due to electrolyte diffusion during charge/discharge, which is quite short in the EIS spectra of sample N-HPC and HPC. This suggests the fast ion transport through the hierarchical porous structure. Fig. 4d shows the cyclic stability of two samples. After 4000 charge/discharge cycles, the N-HPC electrode still retains 86% of its original capacitance, which is higher than 81% of HPC and 72% of YP-17D.

As-obtained N-HPC material is also a quite promising conductive substrate for sulfur loading. In this work, we impregnate sulfur into the hierarchical pores to prepare the N-HPC/S cathode. HPC/S and YP-17D/S composites were also prepared for reference. Fig. 4a shows the XRD patterns of the pristine sublimed sulfur and carbon/sulfur (C/S) composites. The sharp and strong diffraction peaks in sublimed sulfur suggested the well-defined crystal structure. After incorporating sulfur into the porous carbons, the sharp diffraction peaks were significantly weakened. This indicates the highly dispersed state of sulfur inside the porous carbons. We can also observe broad diffraction peaks around 24° in C/S composites which should be assigned to the amorphous characteristics of porous carbons. TGA analysis was carried out to determine the accurate sulfur content in C/S composites and the results

are shown Fig. 4b. We can observe that the TGA curve for YP-17D/S composite shows obviously distinctive two-stage thermal degradation with 200 °C and 300 °C, while it presents only one-stage evaporation process in the TGA curve for N-HPC/S and HPC/S composites. These observations should be ascribed to the different pore structure and thus distinct strength of sulfur adsorption these porous carbons. The porosity of YP-17D mainly comes from micropores, while the sulfur loading of N-HPC and HPC are mostly contributed by mesopores. It is reported that both micropores and mesopores in the carbon matrix can serve a s active sites for sulfur loading, and micropores are believed to enable stronger confinement of sulfurs and therefore higher degradation temperature than mesopores.[29, 41] According to the TGA curves, sulfur contents can be determined to be 76.2 wt%, 70.9 wt% and 62.4 wt% for N-HPC/S, HPC/S and YP-17D/S composites, respectively.

The pore structure of N-HPC/S was also characterized by the nitrogen adsorption test and the resulting adsorption isotherm and corresponding PSD curve are shown in Fig. S6. We can observe that after sulfur impregnation, the porosity of N-HPC/S was enormously reduced. The specific surface area and pore volume of N-HPC/S sharply decrease from 1290 m^2 g^{-1} to 47 m^2 g^{-1}, and from 3.04 cm^3 g^{-1} to 0.42 cm^3 g^{-1}, respectively. From the PSD curve we can see that pores at different pore sizes are all reduced. Especially, the micropores as well as small mesopores with pore size less than 7 nm almost disappeared completely. This implies that sulfur fill in all micropores and small mesopores.

In order to characterize the dispersion of the sulfur particles in the C/S composites,

the SEM images and corresponding elemental mapping of S and C within the composites are shown in Fig. S7. For both N-HPC/S and YP-17D/S composites, we can found no discernible micrometer-size sulfur particles in the SEM images. And a few sulfur nanoparticles can be observed in the YP-17D/S composite. This indicates that the hierarchical porous structure of N-HPC are more beneficial for the homodisperse of the impregnated sulfur. From the elemental mapping we can see that sulfur element dispersed well in all carbon matrixes, which agrees well with the SEM images and the result of the XRD patterns.

To evaluate the electrochemical performance of the C/S composites, coin cells employing lithium foil as an anode and the C/S composite as a cathode were assembled. Fig. 5a shows the CV curves of the N-HPC/S composite at a scan rate of 0.1 mV s^{-1}. In the first scan, two distinctive reduction peaks at 1.95 V and 2.25 V, and one oxidation peak at 2.4 V can be observed. The two remarkable reduction peaks during the cathodic scan should be ascribed to the multistep redox reaction between sulfur and lithium ions. The right reduction peak at 2.25 V is related to the conversion of sulfur to long chain lithium polysulfides (Li_2S_n, $4 \leq n \leq 8$), and the other reduction peak at 1.95 V corresponds to the reduction of lithium polysulfides to Li_2S_2 or Li_2S. The intense oxidation peak during the anodic scan are assigned to the oxidation of Li_2S_2 or Li_2S to high-order lithium polysulfide.[42, 43] In the subsequent two cycles, the reduction peaks shift towards right and the oxidation peak shifts towards left. Thus the voltage difference (ΔE) between the oxidation and reduction peaks grew smaller. Since ΔE represents the potential polarization of the electrode material during

charging/discharging, the lower ΔE values indicate the enhanced electrochemical reversibility [44]. Fig. 5b plots voltages *vs.* specific capacities for the N-HPC/S composite at a charge/discharge rate of 0.2 C. Two discharge plateaus and one charge plateau respectively corresponding to the electrochemical reduction and oxidation of sulfur can be seen. In addition, a low discharge voltage plateaus is demonstrated in the first cycle, which suggests a high polarization level. In the following two cycles, the discharge voltage plateaus are shifted to higher values. The smaller potential separation between the charge and discharge plateaus indicates the improved kinetics characteristics during cycling.[45] These observations are in well agreement with the CV results. According to the discharge curve, a high initial discharge capacity of 1153 mAh g^{-1} can be calculated for the N-HPC/S cathode based on the sulfur mass. Since the sulfur content in N-HPC/S is 76.2%, the discharge capacity based on the total electrode mass can therefore be determined to be as high as 702 mAh g^{-1}. Fig. 7c exhibits the comparison of rate performance between N-HPC/S, HPC/S and YP-17D/S composites. The specific capacities at various charge/discharge current densities from 0.2 C to as high as 4 C were plotted. At 0.2 C, the discharge capacity of N-HPC/S cathode (1153 mAh g^{-1}) is higher than those of HPC/S (1109 mAh g^{-1}) and YP-17D/S (1017 mAh g^{-1}). When the current densities increase to 0.5 C and 1 C, high discharge capacities of 913 mAh g^{-1} and 837 mAh g^{-1} can still be delivered for N-HPC/S cathode. Even at a current density as high as 4 C it still maintains 671 mAh g^{-1}, which is 58.2% of the discharge capacity at 0.2 C. This high-rate performance is much superior to that of YP-17D/S cathode and also better than that of HPC/S. For

HPC/S and YP-17D/S, discharge capacities of 488 mAh g^{-1} and 220 mAh g^{-1} can be delivered at 4 C, respectively. The excellent rate performance of the N-HPC/S cathode is attributed to the highly dispersed sulfur with high electrochemical activity, high electronic conductivity of nitrogen doped porous carbon matrix to facilitate electron transport in the cathode, and the rapid ion transport through the large mesopores inside N-HPC. It is worthwhile mentioning that, the content of sulfur loading shows a great influence on the overall capacity of sulfur/carbon composites, and thus the energy density of Li−S cells.[19] Herein, we also calculated the specific capacities of N-HPC/S cathode based on the total electrode mass at various charge/discharge rates, and compared the data with those of previously reported (as shown in Table. S2). Owing to the high specific capacities based on sulfur mass as well as the high sulfur loading, this work shows among the best reported electrode mass-based rate performances (see Table. S2). It maintains a discharge capacity as high as 409 mAh g^{-1} based on the total electrode mass at 4 C. Fig. 7d shows the cycling stability and of the C/S composites at a current density of 1 C. The N-HPC/S cathode shows a initial discharge capacity of 934 mAh g^{-1}, which is higher than 798 mAh g^{-1} and 542 mAh g^{-1} for HPC/S and YP-17D/S. After 300 charge/discharge cycles, N-HPC/S still remains a high discharge capacity of 600 mAh g^{-1} with 64.2% capacity retention and an average Coulombic efficiency of 99.0%. And the capacity loss per cycle is calculated to be only 0.12%. While the capacity retentions for HPC/S and YP-17D/S are 55.3% and 38.6%, respectively. The cycling performance gap between N-HPC/S and HPC/S demonstrates the strong chemical adsorption of sulfur and polysulfides by

15

nitrogen heteroatoms. Here we also compared the cycling stability with literature reported advanced C/S hybrid systems and the results are summarized in Table S2. We can see that our N-HPC/S composite shows an excellent cycling performance which is among the best reported in the literature.

Conclusions

In summary, we prepared nitrogen-enriched hierarchical porous carbon (N-HPC) through finely controlled pyrolysis of magnesium citrate and subsequent NH_3 treatment. As-prepared N-HPC shows a developed hierarchical micro- and trimodal meso-porosity as well as abundant nitrogen doping. When applied in supercapacitor electrodes, N-HPC shows a specific capacitance of 101 F g^{-1} in nonaqueous electrolyte, which retains 67% even at high current density of 20 A g^{-1}. Such N-HPC material can also be used as an effective carbon matrix for high-content sulfur loading. The N-HPC/S composite cathode shows high discharge capacities of 1153 mAh g^{-1} based on the sulfur mass and 702 mAh g^{-1} based on the total electrode mass at 0.2 C. Superior rate performance can be achieved due to the high sulfur dispersibility, good electric conductivity of N-HPC/S composite and smooth ion transport in large mesopores. Even at a charge/discharge rate as high as 4 C, a large discharge capacity of 671 mAh g^{-1} can be obtained. Moreover, after 300 charge/discharge cycles at 1 C it still remains 600 mAh g^{-1} with a 99.0% Coulombic efficiency. Considering the low cost of raw materials and facile scalable processes, this work features a promising approach to prepare advanced porous carbons for applications in high-performance supercapacitors and Li–S batteries.

16

Acknowledgements

**Appendix A. Supporting Information**

Notes and references

1.   J. R. Miller and P. Simon, *Science*, 2008, **321**, 651-652.

2.   M. F. El-Kady, V. Strong, S. Dubin and R. B. Kaner, *Science*, 2012, **335**, 1326-1330.

3.   M. Winter and R. J. Brodd, *Chem. Rev.*, 2004, **104**, 4245-4270.

4.   X. Ji, K. T. Lee and L. F. Nazar, *Nat. Mater.*, 2009, **8**, 500-506.

5.   S.-E. Cheon, K.-S. Ko, J.-H. Cho, S.-W. Kim, E.-Y. Chin and H.-T. Kim, *J. Electrochem. Soc.*, 2003, **150**, A796-A799.

6.   P. Simon and Y. Gogotsi, *Nat. Mater.*, 2008, **7**, 845-854.

7.   Y. Zhu, S. Murali, M. D. Stoller, K. Ganesh, W. Cai, P. J. Ferreira, A. Pirkle, R. M. Wallace, K. A. Cychosz and M. Thommes, *Science*, 2011, **332**, 1537-1541.

8.   L. F. Nazar, M. Cuisinier and Q. Pang, *MRS Bull.*, 2014, **39**, 436-442.

9.   H. Wang, Y. Yang, Y. Liang, J. T. Robinson, Y. Li, A. Jackson, Y. Cui and H. Dai, *Nano Lett.*, 2011, **11**, 2644-2647.

10.   S. Evers and L. F. Nazar, *Acc. Chem. Res.*, 2012, **46**, 1135-1143.

11.   S. Zhang, L. Chen, S. Zhou, D. Zhao and L. Wu, *Chem. Mater.*, 2010, **22**, 3433-3440.

12.   H. Zhang, Q. Zhu, Y. Zhang, Y. Wang, L. Zhao and B. Yu, *Adv. Funct. Mater.*, 2007, **17**, 2766-2771.

13.   D.-W. Wang, F. Li, G. Q. Lu and H.-M. Cheng, *Carbon*, 2008, **46**, 1593-1599.

14.   D.-W. Wang, F. Li, M. Liu, G. Q. Lu and H.-M. Cheng, *Angew. Chem. Int. Ed.*, 2008, **47**, 373-376.

15. B. Ding, C. Yuan, L. Shen, G. Xu, P. Nie and X. Zhang, *Chem.–Eur. J.*, 2013, **19**, 1013-1019.

16. K. Xi, S. Cao, X. Peng, C. Ducati, R. V. Kumar and A. K. Cheetham, *Chem. Commun.*, 2013, **49**, 2192-2194.

17. Y. Lv, L. Gan, M. Liu, W. Xiong, Z. Xu, D. Zhu and D. S. Wright, *J. Power Sources*, 2012, **209**, 152-157.

18. D. Li, F. Han, S. Wang, F. Cheng, Q. Sun and W.-C. Li, *ACS Appl. Mater. Interfaces*, 2013, **5**, 2208-2213.

19. G.-L. Xu, Y.-F. Xu, J.-C. Fang, X.-X. Peng, F. Fu, L. Huang, J.-T. Li and S.-G. Sun, *ACS Appl. Mater. Interfaces*, 2013, **5**, 10782-10793.

20. G. Srinivas, V. Krungleviciute, Z.-X. Guo and T. Yildirim, *Energy Environ. Sci.*, 2014, **7**, 335-342.

21. J. Schuster, G. He, B. Mandlmeier, T. Yim, K. T. Lee, T. Bein and L. F. Nazar, *Angew. Chem. Int. Ed.*, 2012, **51**, 3591-3595.

22. L. Qie, W. Chen, H. Xu, X. Xiong, Y. Jiang, F. Zou, X. Hu, Y. Xin, Z. Zhang and Y. Huang, *Energy Environ. Sci.*, 2013, **6**, 2497-2504.

23. Z. S. Wu, A. Winter, L. Chen, Y. Sun, A. Turchanin, X. Feng and K. Müllen, *Adv. Mater.*, 2012, **24**, 5130-5135.

24. L.-F. Chen, X.-D. Zhang, H.-W. Liang, M. Kong, Q.-F. Guan, P. Chen, Z.-Y. Wu and S.-H. Yu, *ACS Nano*, 2012, **6**, 7092-7102.

25. X. Wang, Z. Zhang, Y. Qu, Y. Lai and J. Li, *J. Power Sources*, 2014, **256**, 361-368.

26. F. Sun, J. Wang, H. Chen, W. Li, W. Qiao, D. Long and L. Ling, *ACS Appl. Mater. Interfaces*, 2013, **5**, 5630-5638.

27. J. Song, T. Xu, M. L. Gordin, P. Zhu, D. Lv, Y. B. Jiang, Y. Chen, Y. Duan and D. Wang, *Adv. Func. Mater.*, 2014, **24**, 1243-1250.

28. J. Guo, Y. Xu and C. Wang, *Nano Lett.*, 2011, **11**, 4288-4294.

29. X. G. Sun, X. Wang, R. T. Mayes and S. Dai, *ChemSusChem*, 2012, **5**, 2079-2085.

18

30. Y. Qiu, W. Li, W. Zhao, G. Li, Y. Hou, M. Liu, L. Zhou, F. Ye, H. Li and Z. Wei, *Nano Lett.*, 2014, **14**, 4821-4827.

31. X. Yu, C. Zhan, R. Lv, Y. Bai, Y. Lin, Z.-H. Huang, W. Shen, X. Qiu and F. Kang, *Nano Energy*, 2015, **15**, 43-53.

32. M. Inagaki, M. Kato, T. Morishita, K. Morita and K. Mizuuchi, *Carbon*, 2007, **45**, 1121-1124.

33. X. Y. Chen, Y. Y. He, H. Song and Z. J. Zhang, *J. Solid State Electrochem.*, 2015, **19**, 179-186.

34. G. Ferrero, M. Sevilla and A. Fuertes, *Carbon*, 2015, **88**, 239-251.

35. T. Tsumura, A. Arikawa, T. Kinumoto, Y. Arai, T. Morishita, H. Orikasa, M. Inagaki and M. Toyoda, *Mater. Chem. Phys.*, 2014, **147**, 1175-1182.

36. J. Wang, Y. Wu, Z. Shi and C. Wu, *Electrochimica Acta*, 2014, **144**, 307-314.

37. J. Wei, D. Zhou, Z. Sun, Y. Deng, Y. Xia and D. Zhao, *Adv. Func. Mater.*, 2013, **23**, 2322-2328.

38. J. Liang, X. Du, C. Gibson, X. W. Du and S. Z. Qiao, *Adv. Mater.*, 2013, **25**, 6226-6231.

39. H. Chen, F. Sun, J. Wang, W. Li, W. Qiao, L. Ling and D. Long, *J. Phys. Chem. C*, 2013, **117**, 8318-8328.

40. Z. Fan, Y. Liu, J. Yan, G. Ning, Q. Wang, T. Wei, L. Zhi and F. Wei, *Adv. Energy Mater.*, 2012, **2**, 419-424.

41. J. T. Lee, Y. Zhao, S. Thieme, H. Kim, M. Oschatz, L. Borchardt, A. Magasinski, W. I. Cho, S. Kaskel and G. Yushin, *Adv. Mater.*, 2013, **25**, 4573-4579.

42. Y.-X. Wang, L. Huang, L.-C. Sun, S.-Y. Xie, G.-L. Xu, S.-R. Chen, Y.-F. Xu, J.-T. Li, S.-L. Chou and S.-X. Dou, *J. Mater. Chem.*, 2012, **22**, 4744-4750.

43. Y.-S. Su, Y. Fu, T. Cochell and A. Manthiram, *Nat. Commun.*, 2013, **4**, 2985-2992.

44. Z. Sun, M. Xiao, S. Wang, D. Han, S. Song, G. Chen and Y. Meng, *J. Power Sources*, 2015, **285**, 478-484.

45. W. Bao, Z. Zhang, C. Zhou, Y. Lai and J. Li, *J. Power Sources,* 2014, **248**, 570-576.
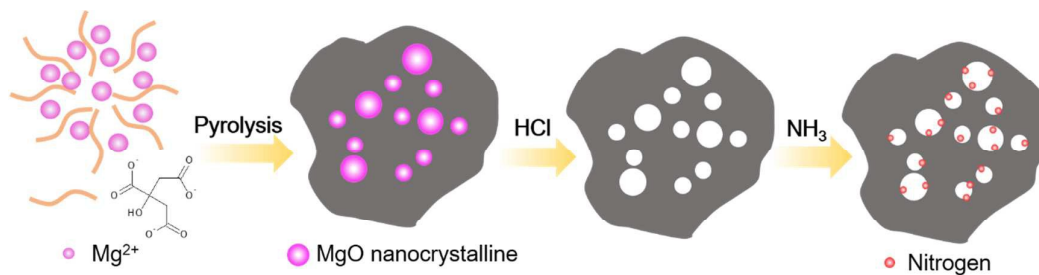
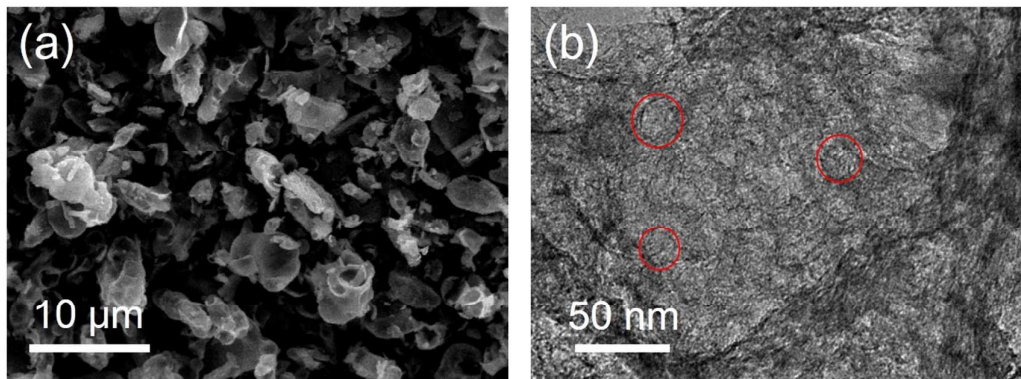Scheme 1 Schematic diagram for the synthesis of sample N-HPC.
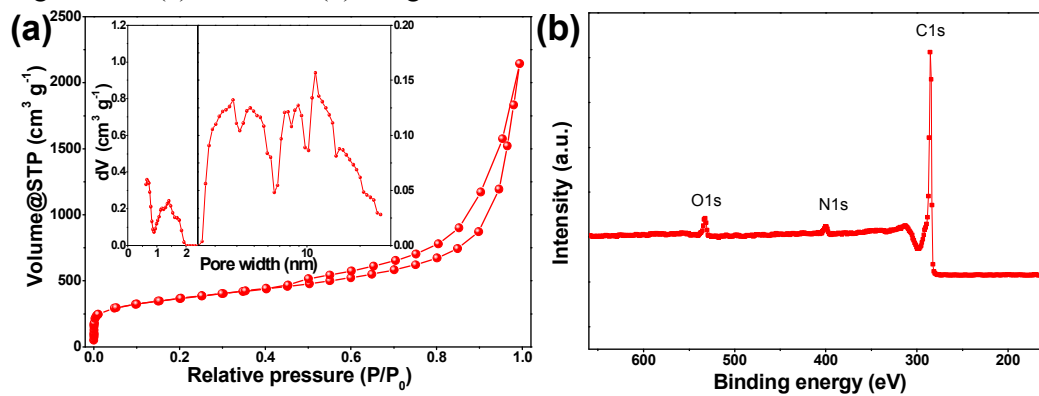

Fig. 1 SEM (a) and TEM (b) images of N-HPC.

Fig. 2 Microstructure properties of sample N-HPC: (a) nitrogen adsorption-desorption isotherms and the corresponding PSD curve (inset); (b) XPS spectrum.
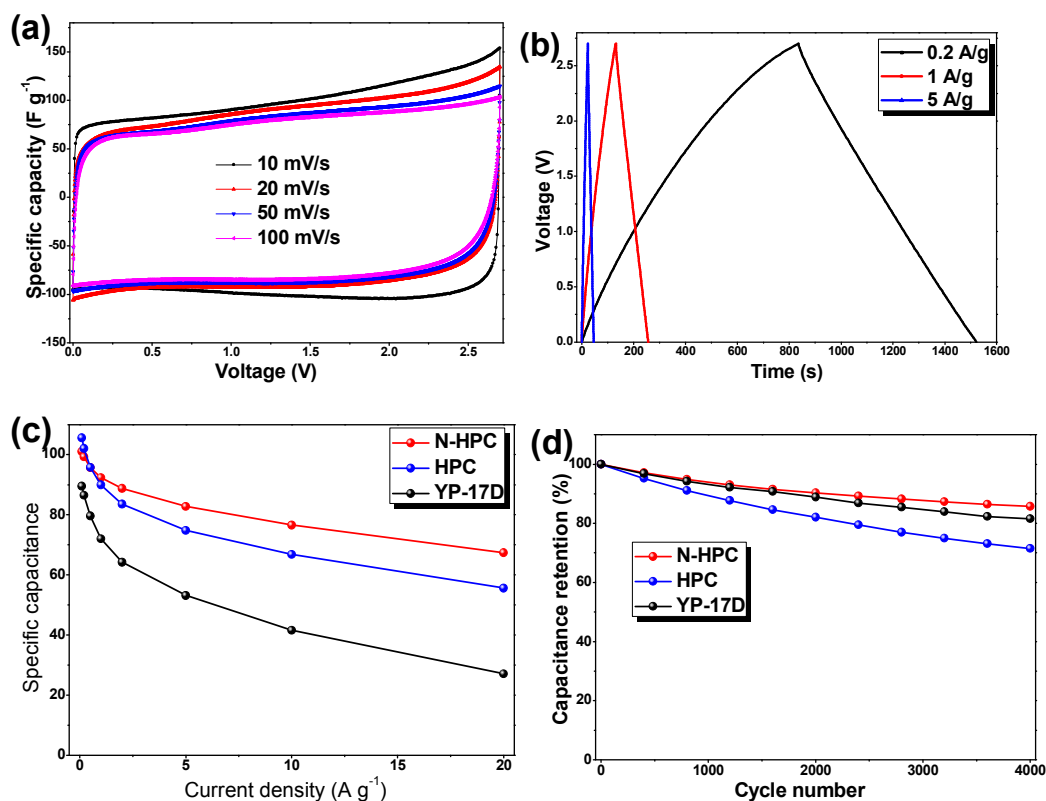
Fig. 3 Electrochemical performances of supercapacitor electrodes based on N-HPC, HPC and YP-17D: (a) CV curves at various scan rates for N-HPC, (b) GC curves at various current densities for N-HPC, (c) rate performances of N-HPC, HPC and YP-17D, (d) cycling stability of N-HPC, HPC and YP-17D.
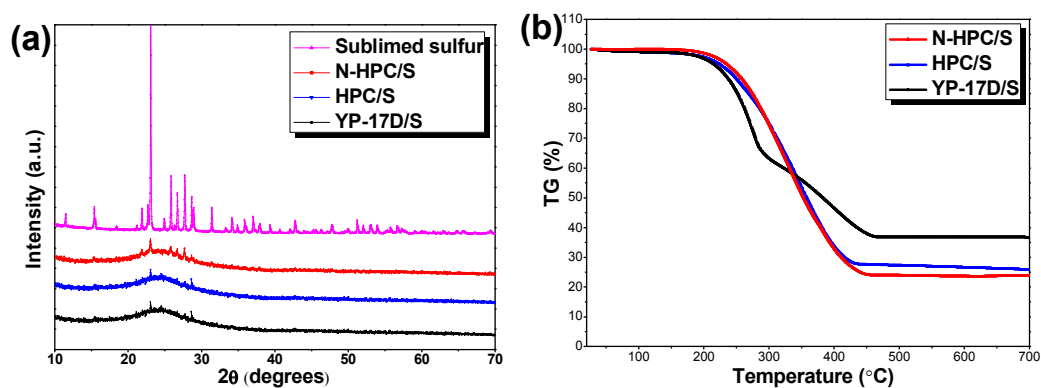

Fig. 4 Microstructure of C/S composites: (a) XRD patterns of C/S composites and pristine sublimed sulfur, (b) TGA curves of C/S composites.
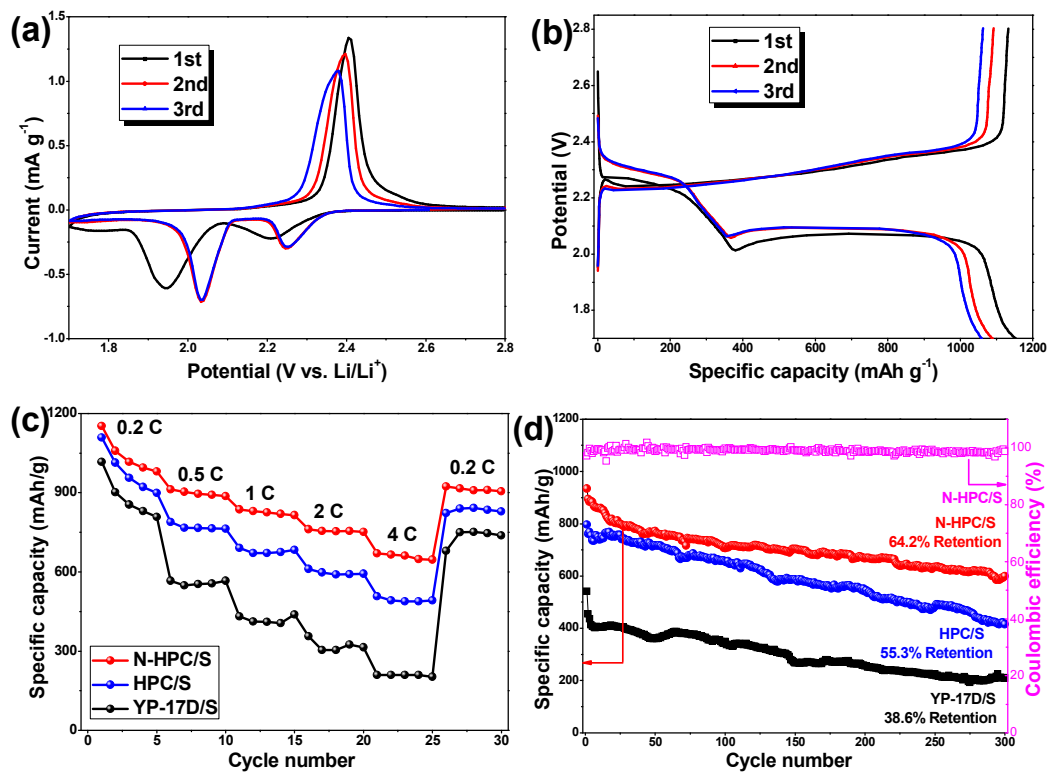
Fig. 5 Electrochemical performances of C/S cathodes: (a) CV curves of N-HPC/S cathode at a scan rate of 0.1 mV s^{-1}, (b) charge and discharge curves of N-HPC/S cathode at a current density of 0.2 C, (c) rate performances of N-HPC/S, HPC/S and YP-17D/S cathodes, (d) cycling stability of the C/S cathodes.